Michele Marconcini
e-mail: michele.marconcini@arnone.de.unifi.it

Filippo Rubechini

Andrea Arnone

"Sergio Stecco" Department of Energy Engineering,
University of Florence,
via di Santa Marta 3,
50139 Firenze, Italy

Seiichi Ibaraki
Nagasaki R&D Center,
Mitsubishi Heavy Industries, Ltd.,
5-717-1 Fukahori-machi,
Nagasaki 851-0392, Japan

Numerical Analysis of the Vaned Diffuser of a Transonic Centrifugal Compressor

A three-dimensional Navier–Stokes solver is used to investigate the flow field of a high pressure ratio centrifugal compressor for turbocharger applications. Such a compressor consists of a double-splitter impeller followed by a vaned diffuser. Particular attention is focused on the analysis of the vaned diffuser, designed for high subsonic inlet conditions. The diffuser is characterized by a complex three-dimensional flow field and influenced by the unsteady interaction with the impeller. Detailed particle image velocimetry flow measurements within the diffuser are available for comparison purposes.
[DOI: 10.1115/1.2988481]

Introduction

In the past decades interest has been increasingly devoted to the development of turbochargers. Because of their compact size, large capacity, high performance, and ability to improve specific fuel consumption, turbochargers are widely used in many applications, such as marine diesel engines, automobile engines, and small gas turbines for aircraft engines.

The requirement for high efficiency and compact size has lead to the widespread use of vaned diffusers in highly loaded transonic centrifugal stages [1–3]. The diffuser is usually subjected to a strong three-dimensional nonuniform unsteady flow discharged from the impeller. In order to achieve higher diffuser performance and to expand the operating range, it is believed that it may be essential to take into account the influence of the impeller flow on the aerodynamic design. To this aim, in the past years considerable attention has been paid to vaned diffuser flow. Various aspects of the impeller diffuser interaction have been addressed both experimentally and numerically (e.g., Refs. [4–12]). Notwithstanding there is still a lack of quantitative understanding in terms of impeller diffuser interaction, and the matching of these components can be a difficult task for the designers. As a matter of fact Cumpsty [1] and Shum et al. [19] state that generally the most common cause of poor performance with high pressure ratio machines is mismatching and not geometrical details of the impeller or diffuser shape.

Krain [13] performed unsteady measurements of the flow in the vaneless space and in the vaned diffuser of a high pressure ratio transonic centrifugal compressor using the laser two focus technique. The analysis showed a highly distorted inlet flow in the spanwise direction and an unsteady fluctuation of about 10 deg in the inlet flow angle with a maximum unsteadiness upstream of diffuser vanes. The unsteadiness decreased aft of the diffuser throat, but experimental data highlighted a large region of low momentum flow that developed near the diffuser pressure side.

Ibaraki et al. [14,15] investigated the flow in a test compressor stage for turbocharger applications, focusing on the double-splitter transonic impeller using laser doppler velocimetry (LDV) technique. The impeller flow of such a compressor was analyzed numerically by Ibaraki et al. [14,15] and Marconcini et al. [16].

Recently Ibaraki et al. [17] conducted particle image velocimetry (PIV) measurements on the vaned diffuser of the same centrifugal compressor stage. They found that the impeller affects the diffuser inlet flow causing a three-dimensional distortion in the spanwise direction. The vaned diffuser flow is strongly unsteady and an inlet angle fluctuation of about 5–10 deg was measured. The mixing of the impeller exit flow was extremely delayed, and the impeller wake is still present downstream of the diffuser throat.

The current study is aimed at analyzing the three-dimensional flow field of the vaned diffuser previously investigated by Ibaraki et al. [17]. Both steady state and unsteady analyses were carried out. The goal was to closely match the operating point near the design flow rate, where detailed time-dependent measurements are available for the diffuser. It is believed that a better understanding of the physical mechanisms, which govern the flow in the vaneless space between the impeller outlet and the diffuser throat, can represent the basis for drawing up design guidelines.

Compressor Stage Description

The compressor stage is composed of a centrifugal impeller with 7 blades and double splitters with 7 and 14 blades, respectively, and a vaned diffuser with 19 blades. The impeller is unshrouded with a tip clearance varying from 0.65 mm at the blade inlet to 1 mm at exit. The size of the radial gap, expressed as the radius ratio of the diffuser leading edge to the impeller trailing edge is $r_3/r_2=1.15$. The diffuser vanes are of the double-circular-arc type and have a constant height equal to the impeller exit width. Figure 1 shows a sketch of the compressor test rig with the transonic impeller and the vaned diffuser followed by a volute, while Table 1 summarizes the main geometrical parameters. The design rotational speed is 24,700 rpm, and pressure ratio is 3.9:1 with a volume flow, referred to as the inlet conditions, of 6.8 m^3/s, leading to an inlet Mach number of about 1.3. The vaned diffuser presents high subsonic inlet conditions with an inlet design Mach number of about 0.95.

Detailed PIV measurements for the vaned diffuser are available; the experimental procedure was described by Ibaraki et al. [17]. Due to test equipment constraints a compressor stage approximately 14% smaller was used, and the impeller peripheral speed was maintained the same as in the previous works [14,15]. Nev-

Contributed by the International Gas Turbine Institute of ASME for publication in the JOURNAL OF TURBOMACHINERY. Manuscript received September 19, 2007; final manuscript received December 3, 2007; published online May 5, 2010. Review conducted by David Wisler. Paper presented at the ASME Turbo Expo 2007: Land, Sea, and Air (GT2007), Montreal, QC, Canada, May 14–17, 2007.

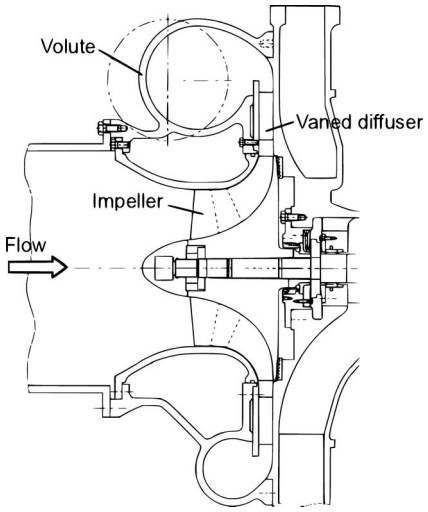

Fig. 1 Cross section of the compressor stage

ertheless the pressure ratio of the scaled stage at the design condition was slightly lower due to scale effect and to the influence of the PIV system [17]. All computations presented in this paper were carried out on the full scale stage geometry. Figure 2 shows the diffuser measurement cross sections in the direction of the vane height, corresponding to Section A at 67% of the vane span, Section B at midspan, and Section C at 23% of the vane span.

Computational Procedure

The multirow multiblock release of the TRAF code developed by Amone [18] was used in the present work. The unsteady three-dimensional Reynolds averaged Navier–Stokes equations are written in conservative form in a curvilinear body-fitted coordinate system and are used to solve for the density, absolute momentum components, and total energy.

Table 1 Compressor stage geometrical data

Impeller	
Blade no.	7+7+14 (double splitter)
Inlet hub diameter	94.6 mm
Inlet tip diameter	261.3 mm
Inlet tip angle	29.8 deg (from tangential)
Exit diameter	373 mm
Exit blade height	23.5 mm
Exit backsweep angle	25 deg
Diffuser	
Blade no.	19
Inlet diameter	429 mm
Inlet angle	21 deg (from tangential)
Exit diameter	590.1 mm

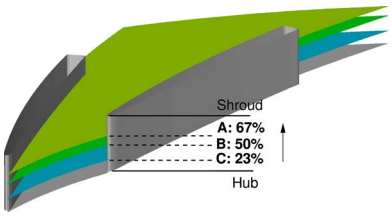

Fig. 2 PIV measurement locations

The code has recently been used for the design and optimization of transonic centrifugal compressor impellers [19,20] and for the analysis of component interaction in centrifugal compressor stages [21,22].

Numerical Scheme. The space discretization is based on a cell-centered finite volume scheme. Both scalar and matrix artificial dissipation models introduced by Jameson et al. [23] and Swanson and Turkel [24] are available in the code. In order to minimize the amount of artificial diffusion inside the shear layers an eigenvalue scaling was implemented to weight these terms. The system of governing equations is advanced in time using an explicit four-stage Runge–Kutta scheme. Residual smoothing, local time stepping, and multigridding are employed to speed-up the convergence to the steady state solution.

Inflow and outflow boundaries are treated according to the theory of characteristics: the flow angles, total pressure, and temperature are imposed at the subsonic first row inlet, while the outgoing Riemann invariant is taken from the interior. At the subsonic last row outlet, static pressure is prescribed, and the density and the momentum components are extrapolated. The link between rows is handled by means of mixing-planes. Consecutive rows have a common interface plane, and the match is provided through the appropriate calculation of phantom cell values, keeping the spanwise distribution while averaging in the blade-to-blade direction.

A dual time stepping method [25,26] is used to perform time accurate calculations. By introducing the dual time stepping concept, the solution is advanced in nonphysical time, and all the acceleration strategies used for the steady computation are exploited to speed up the residual to zero and to satisfy the time-accurate equations. The link between rows is handled by means of sliding interface planes. The phantom cells relative to the interface plane lie on the adjacent blade passage, and linear interpolations are used to provide the flow variable values.

The code features several turbulence closures, namely, the algebraic Baldwin–Lomax model [27], the one-equation Spalart–Allmaras model [28], and the two-equation Wilcox k-ω model [29]. In the present work, the Baldwin–Lomax model was employed.

Computational Grids. The impeller computational domain was divided into four mesh blocks, one for each of the four semivanes included between two main blades. Each of them was discretized using an H-type elliptic grid with $149 \times 41 \times 57$ points in the streamwise, pitchwise, and span-wise directions, respectively. In this way, the total number of mesh cells between two main blades in the pitchwise direction is 160, and the total number of grid points for the impeller is 1,392,852. The value of y^+ for the first grid point above the wall, was between 1.0 and 4.0 for all the blades. For the diffuser vane, a $141 \times 57 \times 57$ single-block H-type grid was adopted.

A three-dimensional view of the computational mesh is shown in Fig. 3. The impeller tip clearance was discretized with 16 cells, the clearance region was handled by pinching the blade (e.g., Ref. [30]), and the tip gap is fully gridded.

Flow Analysis and Discussion

Following the approach suggested by Pierzga and Wood [31], the comparison between calculations and experiments was carried out using the mass flow rate nondimensionalized with the choke mass flow rate as the equivalence criterion. In a transonic compressor rotor this criterion is applied to ensure that the same operating condition is matched by both the experiments and computations.

Figure 4 shows the comparison between measured and computed compressor stage characteristics. For unsteady computations the number of diffuser vanes was modified from 19 to 21. It is common practice in unsteady stage computations to modify the blade count in the rotor and/or stator in order to end up with

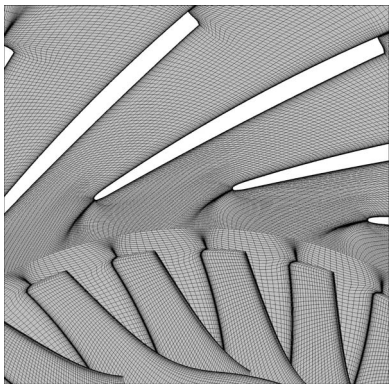

Fig. 3 Three-dimensional view of the impeller and diffuser computational mesh

reasonable memory and CPU time requirements. For this reason unsteady computations were performed on a stage configuration with 7 impeller full blades and 21 diffuser vanes in order to attain the minimum periodicity with one impeller vane composed of four semivanes and three diffuser vanes. The impact of such an alteration on the compressor stage pressure ratio was evaluated by performing a steady computation with 19 and 21 diffuser vanes. Using the steady approach it was not possible to simulate operating conditions close to the compressor stall because unsteady phenomena appear when going toward lower mass flow rates, and the code is not able to converge anymore. The numerical stall limit was considered as the last calculation for which the code converged.

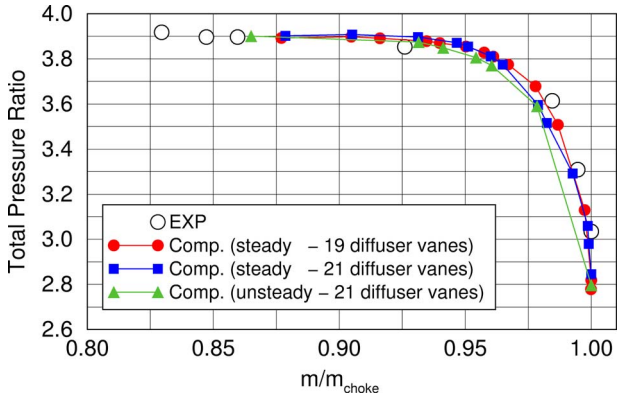

Fig. 4 Compressor stage characteristic (full scale geometry)

Steady Computations

Figure 5 shows the circumferential averaged flow angle and meridional velocity at a diameter 12% downstream of the impeller exit. Looking at Fig. 5(*a*) the computed flow angle at peak efficiency exhibits a large spanwise nonuniformity of about 50 deg. Since the diffuser was designed for an inlet flow angle of 21 deg, negative incidence will be experienced from hub to midspan. Going toward the shroud, the flow angle tends to become tangential and indicates the presence of a back flow region over 85% of the span, due to the wake flow discharged by the impeller. This behavior was observed on the same compressor by Ibaraki et al. [17], as well as in other measurement results (cf. Refs. [3,13]). The measured flow angles from 23% to 67% span differ by about 9 deg at peak efficiency, while computed results give a difference of about 14 deg. Considering the near choke and the near stall conditions, the measured variations are of about 13 deg and 9 deg, respectively, against computed differences of 15 deg and 17 deg.

The magnitude of the reverse flow region is highlighted by the spanwise distribution of the meridional velocity shown in Fig. 5(*b*). The computed velocity distribution near the stall is in good agreement with the measured one in terms of both shape and level. As far as the near stall and the near peak conditions are concerned, measured points exhibit a fairly constant velocity level between the 50% and 67% span not detected by computations.

Figure 6 shows the comparison between the measured and computed flow angle contours on the three PIV experimental sections. Computed flow patterns are in good agreement with experimental ones in all three span heights. In Section A, located at 67% span, the inlet flow angle is close to the diffuser design value. Moving toward the hub the inlet flow angle tends to increase, giving rise to negative incidence, which is particularly evident in Section C (23% span), where a flow separation occurs on the vane pressure side.

Unsteady Computations. As shown in Fig. 4 unsteady computations were performed at various operating conditions. In this section the analysis of unsteady results was focused on the near peak condition where detailed time varying measurements are available.

Starting from a steady state solution as initialization, 200 time steps per impeller blade passing period were used with five subiterations per time step. The nondimensional blade lift coefficient based on the pressure distribution was used to monitor the time-periodic convergence. A good level of periodicity was reached after 30 rotor passing periods, ten more cycles were performed to check the stability of the results. Figure 7(*a*) shows the evolution of the nondimensional lift coefficient amplitude. The more relevant Fourier harmonics were identified for each blade via the lift coefficient spectrum analysis (see Fig. 7(*b*)) and their time evolution to periodicity is plotted over 40 periods for both the impeller and the diffuser blades (Fig. 7(*c*)).

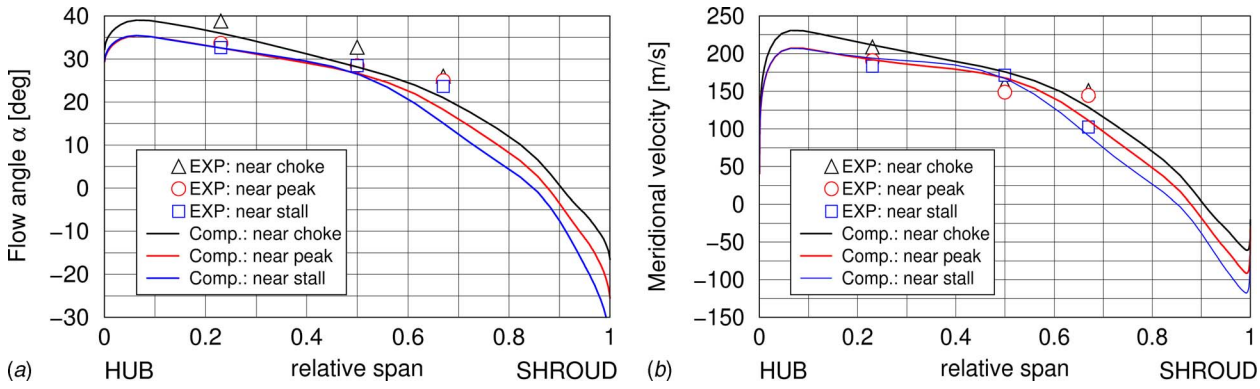

Fig. 5 Measured and computed (steady state) circumferential averaged flow angle (*a*) and meridional velocity (*b*)

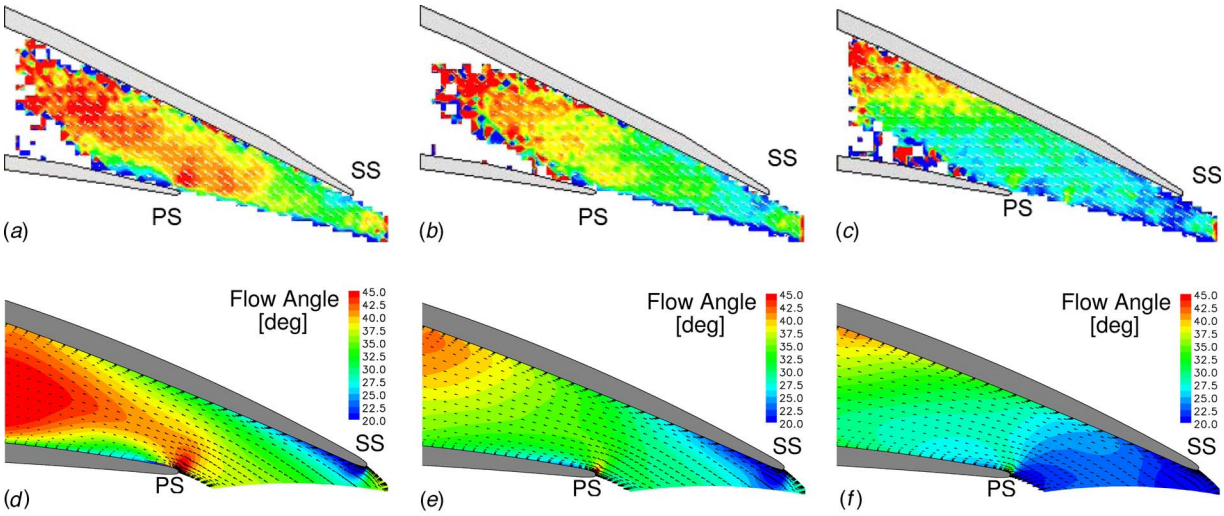

Fig. 6 Comparison between the measured [17] and computed flow angle contours and velocity vectors (near peak): (*a*) Sec. C—23% span (PIV), (*b*) Sec. B—50% span (PIV), (*c*) Sec. A—67% span (PIV), (*d*) Sec. C—23% span, (*e*) Sec. B—50% span, (*f*) Sec. A—67% span

Bearing in mind that for unsteady computations the number of diffuser vanes was altered from 19 to 21, the impact of such an alteration on the spanwise distribution of the pitch-averaged flow angle is shown in Fig. 8. From the two steady computations it is observed that the spanwise shape is modified, resulting in about a 2 deg lower flow angle up to 60% span and a higher flow angle up to 5 deg near the shroud. The time-averaged flow angle slightly differs from the one obtained using the steady approach, probably due to a comparatively large radial gap ($r_3/r_2=1.15$), which tends to attenuate potential flow disturbances (cf. Ref. [8]).

Figure 9(*a*) shows the predicted static pressure rise coefficient C_p at midspan of the diffuser vane. The steady and time-averaged distributions closely match all over the vane surface. Due to the unsteady flow field, at a fixed location of the diffuser surface, pressure is not a constant, but varies cyclically. These fluctuations have been stored for every point of both the suction and pressure sides, and the minimum and maximum C_p registered during a full blade passing period are also reported. A high level of unsteadiness can be appreciated both on the pressure and suction side from the leading edge to the trailing edge. The ratio between the unsteady pressure amplitude and the time-averaged pressure is used to quantify the level of unsteadiness in Fig. 9(*b*). The maximum unsteadiness is detected around the leading edge where values of up to 40% are reached near midspan. A level of unsteadiness varying from 5% to 10% is found on all vane surfaces and a similar pattern is observed from 23% to 67% span.

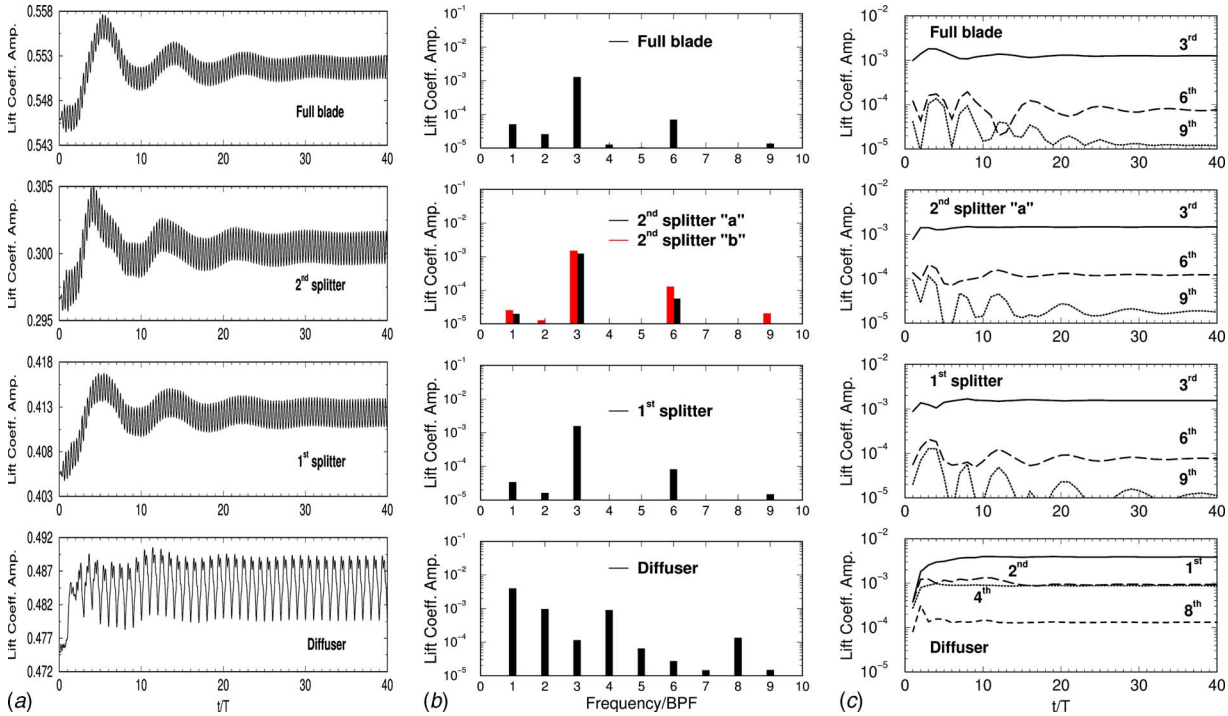

Fig. 7 Evolution of the lift coefficient (*a*) and the lift coefficient amplitude harmonics (*b*) on the impeller (*c*) and on the diffuser blades (near peak)

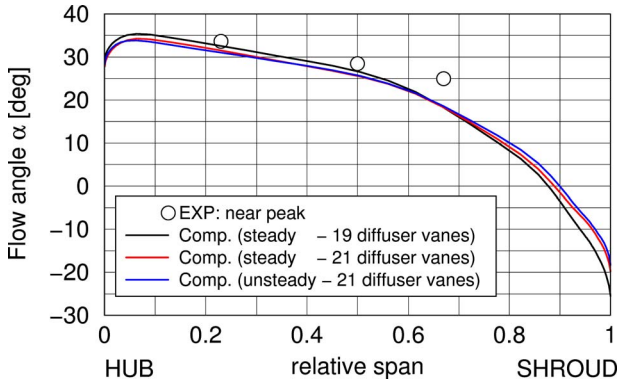

Fig. 8 Measured and computed circumferential averaged flow angle at $r=1.12\cdot r_2$ (near peak)

In Figs. 10(*a*)–10(*c*) the time fluctuations of the flow angle in three positions corresponding to the center of the diffuser vane pitch, and for three different span heights, are shown. Position *a* is located at the diffuser inlet at a radius close to the vane leading edge. Positions *b* and *c* are located near the diffuser throat and downstream of it, respectively. These fluctuations are plotted against a normalized time corresponding to the impeller full blade passing period. Since the impeller has two rows of splitter blades, four wakes associated with the full blade and the splitter blades are observed during the passage of one full blade.

In point *a* (Fig. 10(*a*)) the flow angle undergoes a spanwise variation from 23% to 67% span of about 10 deg. The unsteadiness adds another 5–10 deg from the periodic peak-to-peak angle fluctuation. Compared to position *a*, distributions in the near throat position *b* (Fig. 10(*b*)) exhibit a slightly greater variation in the flow angle, in both the spanwise distortion and the timewise fluctuation. Downstream of the diffuser throat in position *c* (Fig. 10(*c*)) the axial variation of the flow angle from the hub to the shroud is still comparable to the one found in points *a* and *b*,

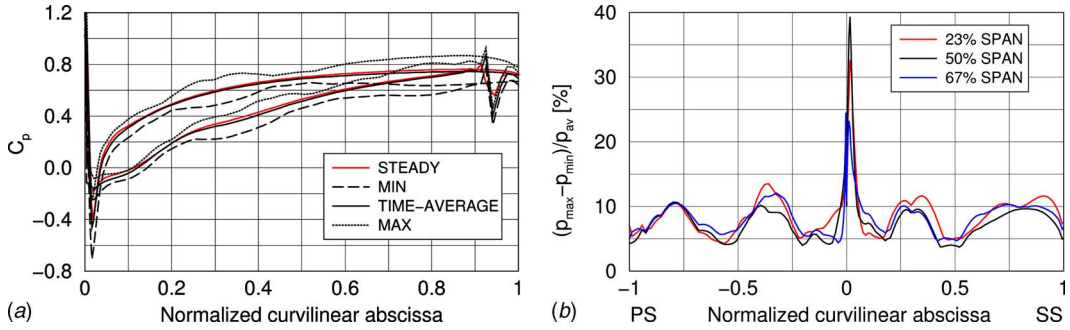

Fig. 9 C_p distributions (*a*) and level of unsteadiness (*b*) on the diffuser vane (near peak)

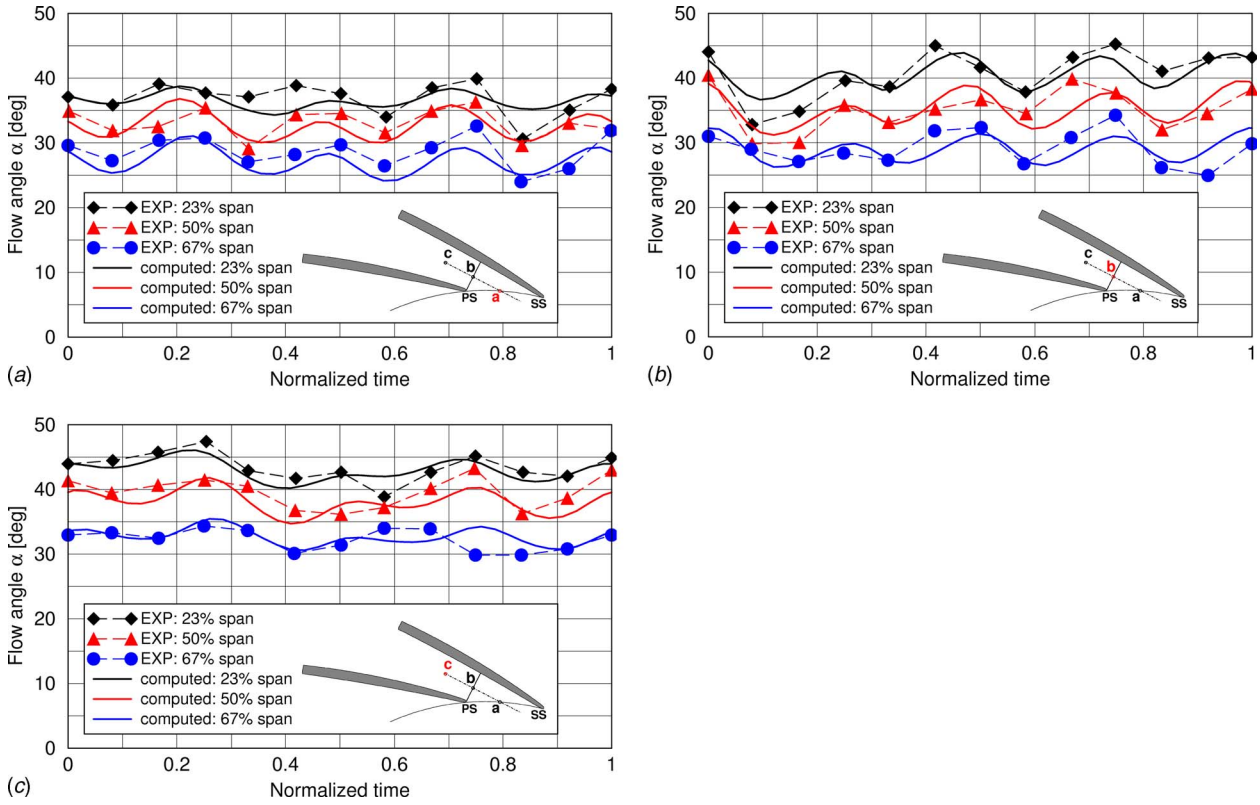

Fig. 10 Time evolution of the flow angle in the vaned diffuser (near peak): (*a*) point *a*, (*b*) point *b*, (*c*) point *c*

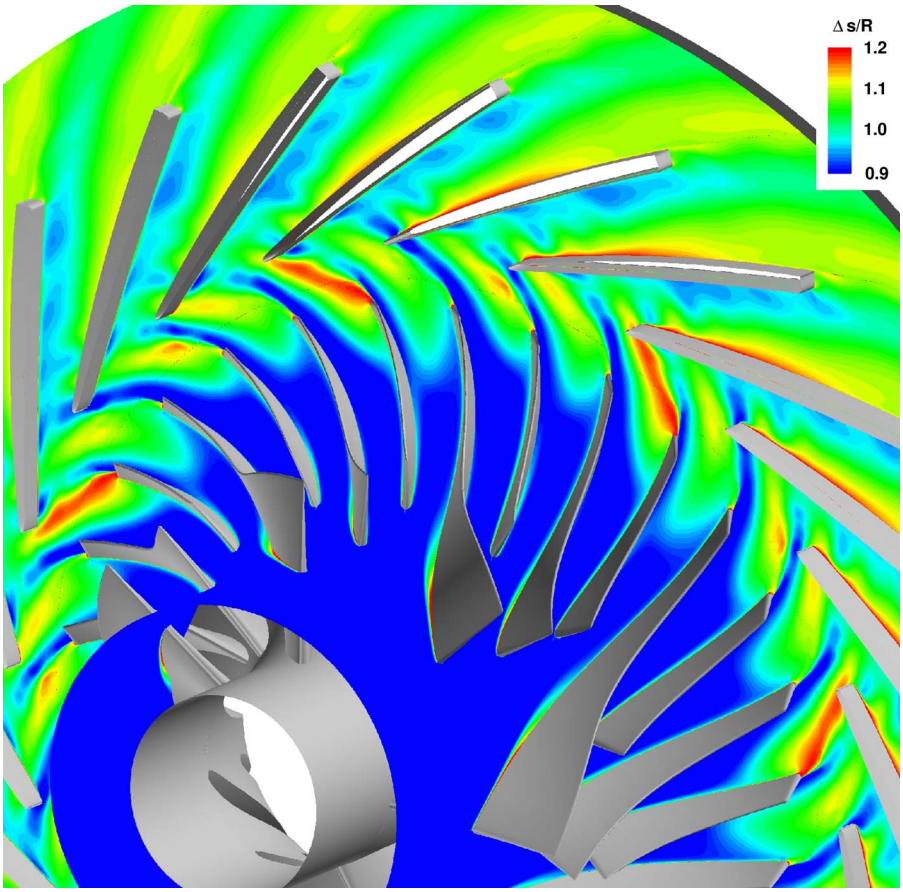

Fig. 11 Instantaneous entropy contours at midspan (near peak)

denoting an extremely delayed mixing in the direction of the vane height. The unsteady fluctuation at 23% and 50% span is again up to 10 deg, while at 67% span it decreases to 5 deg. In all the three considered positions the computed results agree qualitatively and quantitatively with measurements in terms of both the spanwise variations and time evolution.

It has to be remarked that unsteady fluctuations seem to persist well within the diffuser, and this is corroborated by the instantaneous entropy contours near midspan reported in Fig. 11. Here the jet-wake structure of the impeller exit flow is evident. The impeller wakes are chopped by the diffuser vane and can even be identified downstream of the throat without significant diffusion. A similar behavior was confirmed by the unsteady flow angle distributions measured by PIV in the work of Ibaraki et al. [17].

Upstream of the diffuser vanes the time-averaged flow angle spanwise distortion (see Fig. 8) results in a severe incidence distribution along the diffuser height. The high values of the flow angle in the hub region are associated with a negative incidence and a consequent leading edge separation. Many authors have observed that this situation can lead to the development of a large region of low momentum flow on the hub corner close to the vane pressure side, which then undergoes a strong positive pressure gradient resulting in the flow separation (e.g., Refs. [3,13]). This characteristic secondary flow structure was already highlighted by Ibaraki et al. [17] on the same test compressor studied in the present work. On the basis of the PIV measurement results, they predicted that the separation region would vary over time and pulse according to the unsteady incidence fluctuation. In order to investigate this unsteady effect, a closer inspection of the interaction between the passing impeller wakes and the secondary flow structure was carried out. Figures 12(*a*)–12(*j*) show the entropy contours at midspan superposed on the streamlines on the hub and pressure surfaces for ten instants in a blade passing period. The impeller wakes are convected downstream, chopped by the vane leading edge into discrete spots, which remain close to the pressure side, and undergo a substantial mixing well downstream of the throat. Each time a wake impinges the vane leading edge, it causes an increased negative incidence, which is associated with an augmentation of the corner separation. This mechanism is repeated for four times in a given period and can be appreciated at $t/T=0.1$ (Fig. 12(*b*)), $T/t=0.3$ (Fig. 12(*d*)), $T/t=0.6$ (Fig. 12(*g*)), and $T/t=0.8$ (Fig. 12(*i*)), when the chopped wake segments 1–4 have just passed the throat.

In light of such considerations it appears thus to be possible to gain major benefits in improving the diffuser performance through the reduction in incidence and possibly diminishing the positive pressure gradient, which contributes to the formation of the hub corner separation (e.g., Refs. [3,12]).

Summary and Conclusions

A three-dimensional Navier–Stokes solver was used to investigate the vaned diffuser of a high pressure ratio transonic centrifugal compressor for turbocharger applications. Steady state analyses were carried out for the stage with the mixing plane approach for both the original blade count ratio 7:19 and for a modified 7:21 configuration. Unsteady computations were performed on the modified configuration and only a 1:3 ratio was considered in order to reduce CPU and memory resources. The impact of this choice was checked in terms of the stage operating characteristic revealing no major influence. Based on the computed results and comparison with experimental data, the following conclusions are made.

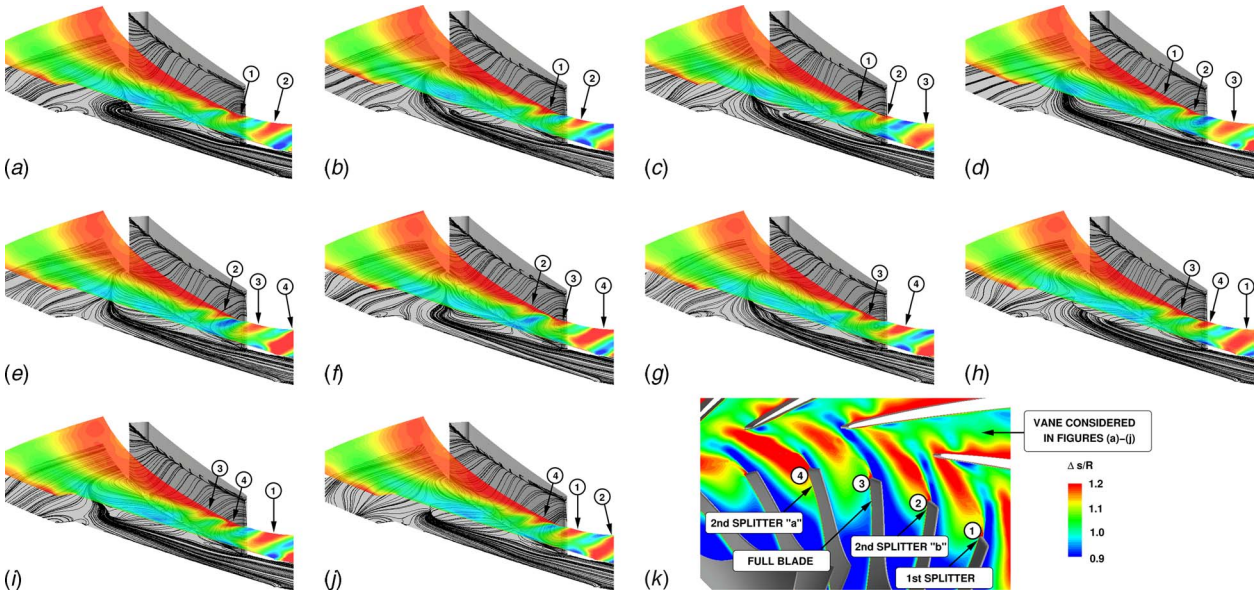

Fig. 12 Instantaneous entropy contours at midspan and the streamline on the hub and pressure surface during an impeller full blade passing period (near peak): (*a*) $t/T=0.0$, (*b*) $t/T=0.1$, (*c*) $t/T=0.2$, (*d*) $t/T=0.3$, (*e*) $t/T=0.4$, (*f*) $t/T=0.5$, (*g*) $t/T=0.6$, (*h*) $t/T=0.7$, (*i*) $t/T=0.8$, (*j*) $t/T=0.9$, and (*k*) wake reference at $t/T=0.0$

- A severe incidence variation was detected at the diffuser inlet in the spanwise direction. Both steady and unsteady computations predicted a flow angle distortion of about 50 deg from the hub to the shroud near peak efficiency. Experimental data qualitatively confirm the shape of the distribution with a variation of about 10 deg from 23% to 67% span. As a result negative incidence is present in the hub region.
- Unsteady computations confirmed the periodic flow unsteadiness observed by the experiments in the diffuser inlet region with temporal variations of the inlet flow angle in the order of 5–10 deg. Flow angle fluctuations seem to persist well within the diffuser vane and can be still detected downstream of the throat where the impeller wakes are scarcely mixed out.
- The flow field analysis in the diffuser passage was conducted by correlating the passing wakes to the pulsating hub-pressure side corner separation triggered by the excessive negative incidence. The physical mechanism associated with the observed flow structures was identified through instantaneous particle path visualization.
- The good agreement between the numerical and the experimental data sustains the fact that most of the interaction effects could be captured, and unsteady computations can represent a reliable tool for investigating the flow development in centrifugal stages thus giving a valid support for the design process.

Acknowledgment

The authors gratefully acknowledge Mitsubishi Heavy Industries Ltd. and, in particular, Mr. Yuichiro Hirano and Mr. Atsushi Matsuo for providing information about the experimental data.

Nomenclature

C_p = static pressure rise coefficient ($C_p=(p-p_3)(p_{t3}-p_3)$)
$\dot{m}$ = mass flow
PS = pressure surface
p = pressure
r = radius
SS = suction surface
T = period
t = time

Greek

α = absolute flow angle (from circumferential direction)

Subscripts

1 = impeller inlet
2 = impeller exit
3 = diffuser inlet
t = total value

References

[1] Cumpsty, N. A., 1989, *Compressor Aerodynamics*, Longmann Scientific and Technical, Essex, England.
[2] Hayami, H., 2000, "Improvement of the Flow Range of Transonic Centrifugal Compressors With a Low-Solidity Cascade Diffuser," *ASME Turbo Expo*, Munich, Germany, May 8–11, ASME Paper No. 2000-GT-465.
[3] Zangeneh, M., Vogt, D., and Roduner, C., 2002, "Improving a Vaned Diffuser for a Given Centrifugal Impeller by 3D Inverse Design," ASME Paper No. 2002-GT-30621.
[4] Inoue, M., and Cumpsty, N. A., 1984, "Experimental Study of Centrifugal Impeller Discharge Flow in Vaneless and Vaned Diffuser," ASME J. Eng. Gas Turbines Power, **106**(2), pp. 455–467.
[5] Hunziker, R., and Gyarmathy, G., 1994, "The Operational Stability of a Centrifugal Compressor and Its Dependence on the Characteristics of the Subcomponents," ASME J. Turbomach., **116**(2), pp. 250–259.
[6] Filipenco, V. G., Deniz, S., Johnston, J. M., Greitzer, E. M., and Cumpsty, N. A., 2000, "Effects of Inlet Flow Field Conditions on the Performance of Centrifugal Compressor Diffuser: Part 1—Discrete-Passage Diffuser," ASME J. Turbomach., **122**(1), pp. 1–10.
[7] Deniz, S., Greitzer, E. M., and Cumpsty, N. A., 2000, "Effects of Inlet Flow Field Conditions on the Performance of Centrifugal Compressor Diffuser: Part 2—Straight-Channel Diffuser," ASME J. Turbomach., **122**(1), pp. 11–21.
[8] Sato, K., and He, L., 2000, "A Numerical Study on Performances of Centrifugal Compressor Stages With Different Radial Gaps," ASME Paper No. 2000-GT-462.
[9] Shum, Y. K. P., Tan, C. S., and Cumpsty, N. A., 2000, "Impeller-Diffuser Interaction in a Centrifugal Compressor," ASME J. Turbomach., **122**(4), pp. 777–786.
[10] Peeters, M., and Sleiman, M., 2000, "A Numerical Investigation of the Unsteady Flow in Centrifugal Stages," ASME Paper No. 2000-GT-426.
[11] Ziegler, K. U., Gallus, H. E., and Niehuis, R., 2003, "A Study on Impeller-Diffuser Interaction—Part I: Influence on the Performance," ASME J. Turbomach., **125**(1), pp. 173–182.
[12] Ziegler, K. U., Gallus, H. E., and Niehuis, R., 2003, "A Study on Impeller-Diffuser Interaction—Part II: Detailed Flow Analysis," ASME J. Turbomach., **125**(1), pp. 183–192.

[13] Krain, H., 2002, "Unsteady Diffuser Flow in a Transonic Centrifugal Compressor," Int. J. Rotating Mach., **8**(3), pp. 222–231.
[14] Ibaraki, S., Higashimori, H., and Matsuo, T., 2001, "Flow Investigation of a Transonic Centrifugal Compressor for Turbocharger," *23rd CIMAC Congress Proceedings*, Hamburg, Germany, May 7–10, pp. 339–346.
[15] Ibaraki, S., Matsuo, T., Kuma, H., Sumida, K., and Suita, T., 2003, "Aerodynamics of a Transonic Centrifugal Compressor Impeller," ASME J. Turbomach., **125**(2), pp. 346–351.
[16] Marconcini, M., Rubechini, F., Arnone, A., and Ibaraki, S., 2008, "Numerical Investigation of a Transonic Centrifugal Compressor," ASME J. Turbomach. **130**(1), p. 011010.
[17] Ibaraki, S., Matsuo, T., and Yokoyama, T., 2007, "Investigation of Unsteady Flow Field in Vaned Diffuser of a Transonic Centrifugal Compressor," ASME J. Turbomach., **129**(4), pp. 686–693.
[18] Arnone, A., 1994, "Viscous Analysis of Three-Dimensional Rotor Flow Using a Multigrid Method," ASME J. Turbomach., **116**(3), pp. 435–445.
[19] Arnone, A., Bonaiuti, D., Ermini, M., Milani, A., and Baldassarre, L., 2003, "Development of a Procedure for the Aerodynamic Design of Transonic Centrifugal Compressor Impellers," *Proceedings of the Fifth European Turbomachinery Conference*, Prague, Czech Republic, Mar. 17–21.
[20] Bonaiuti, D., Arnone, A., Ermini, M., and Baldassarre, L., 2006, "Analysis and Optimization of Transonic Centrifugal Compressor Impellers Using the Design of Experiments Technique," ASME J. Turbomach., **128**(4), pp. 786–797.
[21] Bonaiuti, D., Arnone, A., Hah, C., and Hayami, H., 2002, "Development of Secondary Flow Field in a Low Solidity Diffuser in a Transonic Centrifugal Compressor Stage," *ASME Turbo Expo*, Amsterdam, The Netherlands, Jun. 3–6, ASME Paper No. 2002-GT-30371.
[22] Bonaiuti, D., Arnone, A., Milani, A., and Baldassarre, L., 2003, "Aerodynamic Analysis of a Multistage Centrifugal Compressor," *ASME Turbo Expo*, Atlanta, GA, Jun. 16–19, ASME Paper No. 2003-GT-38495.
[23] Jameson, A., Schmidt, W., and Turkel, E., 1981, "Numerical Solutions of the Euler Equations by Finite Volume Methods Using Runge–Kutta Time-Stepping Schemes," *14th Fluid and Plasma Dynamics Conference*, Palo Alto, CA, Jun. 23–25, AIAA Paper No. 81-1259.
[24] Swanson, R. C., and Turkel, E., 1992, "On Central-Difference and Upwind Schemes," J. Comput. Phys., **101**, pp. 292–306.
[25] Jameson, A., 1991, "Time Dependent Calculations Using Multigrid With Applications to Unsteady Flows Past Airfoils and Wings," *Tenth Computational Fluid Dynamics Conference*, Honolulu, HI, Jun., AIAA Paper No. 91-1596.
[26] Arnone, A., and Pacciani, R., 1996, "Rotor-Stator Interaction Analysis Using the Navier–Stokes Equations and a Multigrid Method," ASME J. Turbomach., **118**(4), pp. 679–689.
[27] Baldwin, B. S., and Lomax, H., 1978, "Thin Layer Approximation and Algebraic Model for Separated Turbulent Flows," *16th Aerospace Sciences Meeting*, Huntsville, AL, Jan. 16–18, AIAA Paper No. 78-257.
[28] Spalart, P. R., and Allmaras, S. R., 1994, "A One-Equation Turbulence Model for Aerodynamic Flows," Rech. Aerosp., **1**, pp. 5–21.
[29] Wilcox, D. C., 1998, *Turbulence Modeling for CFD*, 2nd ed., DCW Industries Inc., La Cañada, CA.
[30] Storer, J. A., and Cumpsty, N. A., 1991, "Tip Leakage Flow in Axial Compressors," ASME J. Turbomach., **113**(2), pp. 252–259.
[31] Pierzga, M. J., and Wood, J. R., 1985, "Investigation of the Three-Dimensional Flow Field Within a Transonic Fan Rotor: Experiment and Analysis," ASME J. Turbomach., **107**(2), pp. 436–449.